Computational study of laser-induced heating of PVDF/nAl composites

Daniel Olsen ; Kyle Uhlenhake ; Mateo Gomez ; Metin Örnek ; Steven F. Son ; Min Zhou ✉

Check for updates

CrossMark

View Online

Export Citation

Computational study of laser-induced heating of PVDF/nAl composites

View Online   Export Citation   CrossMark

Daniel Olsen,[1] [iD] Kyle Uhlenhake,[2] [iD] Mateo Gomez,[2] [iD] Metin Örnek,[2] [iD] Steven F. Son,[2,3] [iD]
and Min Zhou[1,a] [iD]

AFFILIATIONS

[1] School of Mechanical Engineering, School of Materials Science and Engineering, Georgia Institute of Technology, 801 Ferst Dr.,
  Atlanta, Georgia 30332-0405, USA

[2] Purdue University, 500 Allison Road, West Lafayette, Indiana 47907, USA

[3] Purdue Energetics Research Center, Purdue University, West Lafayette, Indiana 47906, USA

[a] Author to whom correspondence should be addressed: min.zhou@gatech.edu

ABSTRACT

Optical sources such as lasers provide a means for precise temporal and spatial control of the ignition of energetic materials through customized deposition of excitation energy. Using coupled microscale electromagnetic (EM) and thermal simulations, we analyze the interactions between the EM waves and the microstructures of PVDF/nAl composites with weight fractions of nAl particles (or solids loadings), w_f, ranging from 10 to 40 wt. %. Statistically equivalent microstructure sample sets with multiple random microstructure instantiations are generated and used for each solid loading, thereby allowing the statistical variations in the material heating behavior due to microstructure randomness to be analyzed. Maxwell's equations are solved to characterize the interactions between the materials and EM waves at wavelengths of 266, 532, and 1064 nm. The resulting energy deposition rate is calculated, accounting for Joule heating, dielectric heating, and magnetic induction heating. The coupled thermal analysis accounts for the energy deposition and thermal diffusion, yielding the temperature fields in the materials. The energy deposition and heating are characterized using three measures: the skin depth of the EM wave, the depth of the significant temperature increase in the material, and the average temperature. An empirical relation is developed for the average temperature increase in the heated layer of the material as a function of the intensity of the input laser, solids loading, and time. It is found that trends in the average temperature and depth of significant heating correlate well with the ignition trends observed in experiments.

INTRODUCTION

Precise control of the ignition of energetic materials requires understanding of the ignition process as well as how materials respond to the source of energy used to cause the ignition. Electromagnetic (EM) waves are a method for ignition that can provide greater control over the rate, magnitude, and spatial positioning of the energy input. Experiments performed by Uhlenhake et al.[1] have shown that the ignition of PVDF/nAl composites under laser and broadband flash excitation can be controlled by tuning the laser input in terms of both intensity and frequency. The microstructure of the material plays an important role in the process. Specifically, it is found that the aluminum content in the material significantly

affects the minimum input energy (MIE) required for ignition. While the experiments clearly demonstrate trends, they do not explain why. Computational simulation can offer an in-depth look at the response of individual microstructure constituents to the incident electromagnetic (EM) waves and the heating process inside the material in ways not feasible experimentally. More importantly, systematic quantification and delineation can also be obtained.

There have been computational studies of the ignition of energetic materials under EM wave excitation. Perry and Duque and Kort-Kamp et al.[2,3] analyzed the heating of HMX in EM fields at microwave frequencies. The studies focused on understanding the areas in the materials with significant temperature increases and the critical conditions for reaction initiation. They showed that the

temperature gradient within the material is heavily dependent on material geometry as well as the local material constituents. Neither studies included aluminum or other conducting particles. Because aluminum is a common additive in energetic materials with unique EM properties, it is critical that further simulations consider aluminum. Although aluminum particles have little interaction with EM waves at microwave frequencies,[4] they can significantly affect the heating process at frequencies in the visible range. A study of the impact of electric fields on aluminum particles has shown that at the lower wavelengths of visible and IR spectra, it is possible to have aluminum particles and EM wave interactions.[5–7] These interactions contribute to both thermal absorption and the plasmonic effect, where the surface electrons interact with EM waves to induce a current.[8] The aluminum particle interactions not only provide sources of heat but also affect the propagation of EM waves into a material, thereby influencing the depth of wave penetration or the skin depth (δ).[9,10] Increasing the amount of particles in a material reduces wave penetration and in turn lowers the amount of material that can receive energy, resulting in more localized surface heating.

Systematically quantifying optical deposition of energy into aluminum-containing materials is of interest in order to better understand the mechanisms behind ignition and identify optimum ignition conditions. Jin *et al.*[11] developed a model for laser ignition of aluminum particles of different sizes that accounted for the effects of oxide shell thickness, porosity, and combustion characteristics. Other models have focused on plasmonic effects as the main contributor to nAl's optical sensitivity. Localized surface plasmon resonance is the resonant oscillation of free electrons in the metals that can confine or enhance the radiation energy absorbed from light sources. These effects are specifically prominent in nanostructures smaller than the light wavelengths interacting with them, and multiple studies have shown aluminum nanoparticles to exhibit these interactions.[5–7] Experimentally, the plasmonic effect is difficult to identify. The plasmonic effect for nAl particles is significant for wavelengths of 200–300 nm, therefore having a pronounced impact on the heating of nAl particle based composites. In addition, experimental work has identified the thermal absorption of nAl particles as one of the leading factors for optical ignition.[1] This is because nAl particles are highly absorption dominated compared to micro-sized aluminum particles, which are scattered or reflection dominated.[12]

In this study, PVDF/nAl films are excited with lasers at wavelengths of 266, 532, and 1064 nm. The resulting field in the material and the deposited energy are analyzed. The deposited energy is used to calculate the temperature increase in the material. The effects of solids loading on the total energy absorbed, temperature distribution in the material, and ignition trends are analyzed.

METHODS

Background experiments

The computational study carried out here is based on a previously-reported set of experiments[1] in which two-gram (2 g) batches of nAl/PVDF mixtures were prepared using nAl particles and PVDF. The films have thicknesses of 35.8 ± 2.6 μm and are cut

into 1 cm^2 square samples. For all ignition experiments, the laser is fired using a pulse burst profile with 5 ms pulses at a rate of 100 kHz. Three wavelengths are considered: 266, 532, and 1064 nm. Due to the physical limitations of the laser at the 266 nm wavelength, the highest applied intensity is 0.8 J/cm^2. A high-speed camera and a photodiode are used to capture ignition and the burning rate, as well as establishing the ignition "go"/"no go" condition, which is used to determine the ignition threshold. A "go" condition is defined as the material continuing to react after the laser pulse has ended. A "no go" event is that the material either never ignites or extinguishes by itself after the laser input ends. The minimum applied laser intensity required to achieve a "go" condition is defined as the minimum ignition energy (MIE). The MIE is 0.6–0.7 J/cm^2 for the 532 nm and the 1064 nm wavelengths. Due to the relatively low power output of the 266 nm wavelength laser, no ignition event is obtained at this wavelength, with applied intensities of up to 0.8 J/cm^2. A more powerful laser is needed to obtain ignition. This result suggests that the material is less absorbent of the EM waves at this lower wavelength than at the higher wavelengths. This observation serves as a useful reference point for the computational study to come.

Materials

The nAl/PVDF composites studied contain a polyvinylidene fluoride (PVDF) matrix or binder and aluminum particles consisting of an Al-core and an Al$_2$O$_3$-shell. The composites have six levels of aluminum by weight, i.e., 10, 15, 20, 25, 30, and 40 wt. %. Figure 1 shows the SEM images of the microstructures with 10 and 30 wt. % Al. The average radius of the particles is ~30 nm, and each particle has a 70 wt. % active aluminum core and a 30 wt. % passivated Al$_2$O$_3$ shell on the outside. The particles are randomly distributed within the material, although the 10 wt. % samples show some agglomeration.

The computational models are generated to capture the overall statistical attributes of the materials, including particle size distribution, content of active aluminum, and random nature of spatial distribution. The Al-core and the Al$_2$O$_3$-shell structure of the particles are explicitly resolved. The nano-sized core-shell particles are circular in shape. The Al core radius ranges from 25 to 35 nm and constitutes 70 wt. % of the core–shell structure. The Al$_2$O$_3$ shell is ~3 nm in thickness. The rest of the microstructures are occupied by PVDF. PVDF and Al$_2$O$_3$ are dielectric and have practically negligible electrical conductivity. Aluminum is electrically conductive. All material properties used are taken from experimental reports in the literature and are listed in Table I.

A total of seven solids loadings between 10% and 40% at an increment of 5% are considered, as shown in Fig. 2. For each case, a statistically equivalent microstructure sample set (SEMSS) with five random samples is used to capture the statistical distributions of the material heterogeneities and response results.

The microstructure samples are 5 × 5 μm^2 in size and are regarded as sufficiently large representative volume elements of the material in the experiments. The model allows the mechanisms and extent of heating to be efficiently analyzed with readily available computational resources.
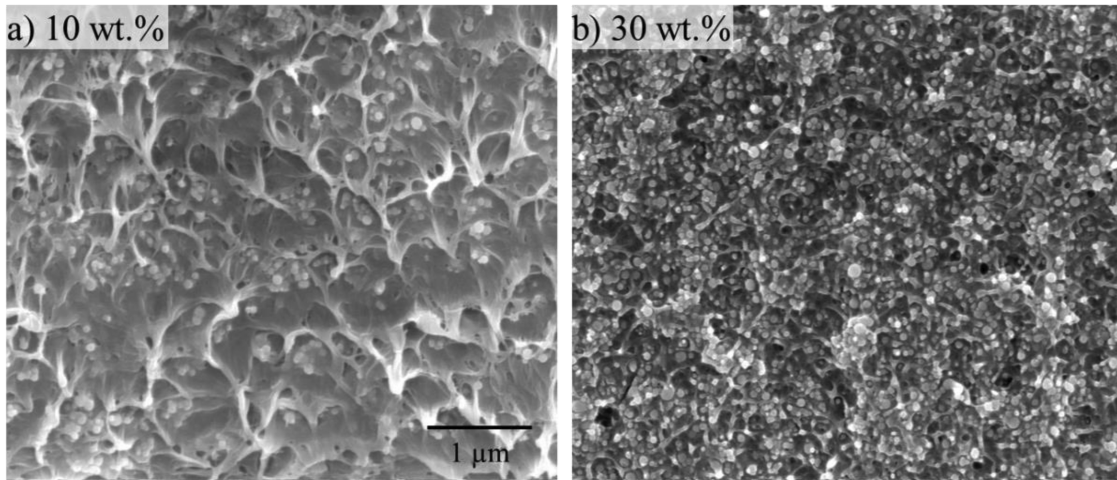
FIG. 1. Microstructures of nAl/PVDF films used in experiments: (a) 10 wt. % and (b) 30 wt. % of aluminum nanoparticles.

Finite element framework

The computation takes place in COMSOL Multiphysics®. The simulations account for the interactions between the EM waves and the constituents in the materials, allowing the electric and magnetic fields, heat generation, thermal conduction, and temperature increases to be explicitly evaluated. The focus is on how heating occurs through the interactions of the electric and magnetic fields (E-field and M-field) of the incident radiation with the composite microstructures with dielectric and conductive constituents. The incident EM waves have intensities in the range of 0.2–2 J/cm and at wavelengths of 266, 532, and 1064 nm. The governing equations for the electrodynamic process are the Maxwell equations in the form of

$$\begin{cases} \nabla \times \mathbf{H} = \dfrac{\partial D}{\partial t} + \mathbf{J}, \\ \nabla \times \mathbf{H} = -\dfrac{\partial \mathbf{B}}{\partial t}, \\ \nabla \cdot \mathbf{B} = 0, \\ \nabla \cdot \mathbf{D} = \rho_c, \end{cases} \tag{1}$$

where

$$\begin{aligned} \mathbf{B} &= \mu \mathbf{H}, \\ \mathbf{D} &= \varepsilon \mathbf{E}, \\ \mathbf{J} &= \sigma \mathbf{E} \cdot \end{aligned} \tag{2}$$

In the above-mentioned relations, $\mathbf{H}$ is the magnetic field intensity, $\mathbf{B}$ is the magnetic induction, $\mathbf{J}$ is the current intensity, μ is the permeability, $\mathbf{E}$ is the electric field intensity, $\mathbf{D}$ is the electric displacement field, and ρ_c is the charge density.

Heat generation and conduction are considered via the conservation of energy relation in the form of

$$\rho_M C_p \frac{\partial T}{\partial t} + \kappa \nabla^2 T = q, \tag{3}$$

where ρ_M is the mass density, C_p is the specific heat under constant pressure, T is the temperature, κ is the thermal conductivity, and q is the heat generation rate per unit volume due to conductive and dielectric dissipation. Note that

$$q = \frac{1}{2}\sigma|\mathbf{E}|^2 + \frac{1}{2}\omega\varepsilon_0\varepsilon''|\mathbf{E}|^2 + \frac{1}{2}\omega\mu_0\mu''|\mathbf{H}|^2, \tag{4}$$

where ε'' is the imaginary part of the complex permittivity, σ is the electrical conductivity, ω is the frequency, and μ'' is the imaginary part of the complex permeability. The first term represents conductive joule heating, the second term represents dielectric heating, and the third term represents magnetic heating. The heat generation rate can be used to obtain the deposited accumulative heat Q in a volume V of a sample up to time t via

$$Q = \int_0^t \int_V q \, dV dt. \tag{5}$$

This quantity is used to assess the heating in different material cases.[16] Trunov *et al.*[17] noted that for ignition to occur, the external

TABLE I. Material properties.

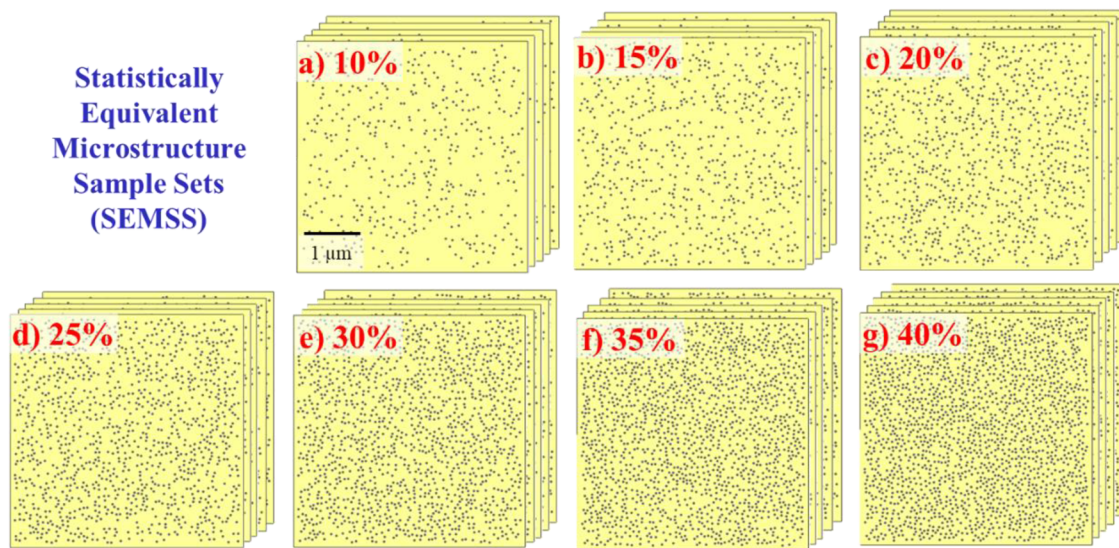| Properties	nAl[13]	Al$_2$O$_3$[13]	PVDF[14,15]
Mass density, ρ_M (kg/m^3)	2941	3970	1780
Relative permittivity, ε	1	9.6–0.0006j	7–0.0009j
Relative permeability, μ	1	1	1
Electrical conductivity, σ (S/m)	3.75×10^7	1×10^{-14}	1×10^{-10}
Specific heat, C_p J/(kg K)	900	765	1200
Thermal conductivity, κ W/(m K)	237	36	0.19

FIG. 2. Statistically equivalent microstructure sample sets (SEMSS) of PVDF/nAl. Each set has five samples with an Al fraction of (a) 10 wt. %, (b) 15wt. %, (c) 20 wt. %, (d) 25 wt. %, (e) 30 wt. %, (f) 35 wt. %, and (g) 40%.

energy input should be higher than the energy loss due to thermal conduction and endothermic chemical processes. This is a necessary condition.

The simulations follow two steps. First, the E-field history in the microstructure is evaluated. The resulting heating rate is calculated using Eq. (4). Subsequently, the temperature field is obtained by solving Eq. (3). The effect of the incident laser beam is accounted for by specifying the alternating E-field at the top edge of the microstructure in Fig. 1 over the duration of desired exposure. The simulations are inert and focus on how energy deposition is affected by the microstructure and solids loading in order to understand the trends observed in the experiments.

A mesh convergence study is performed. The smallest constituents are the nAl particles, which have a minimum radius of 25 nm. The finite element mesh consists of triangular elements, which are 5 nm in size, resulting in ~14 elements across each

particle. The results show that the difference in the electric field for the shortest wavelength of 532 nm using 5 nm elements and 2 nm elements is less than 1%, suggesting that the chosen element size provides sufficient accuracy.

RESULTS

A systematic study of the electric field interaction with the constituents, the temperature increases, and the cumulative energy deposition within each sample is performed. The discussion below focuses on both the magnitudes and the trends of these effects.

The incident wave is partly reflected and partly transmitted into the material. The transmitted part induces the E-field and M-field. Figure 3 shows the E-field distribution for one sample in the statistical sample sets for three different solids loadings (or frac-
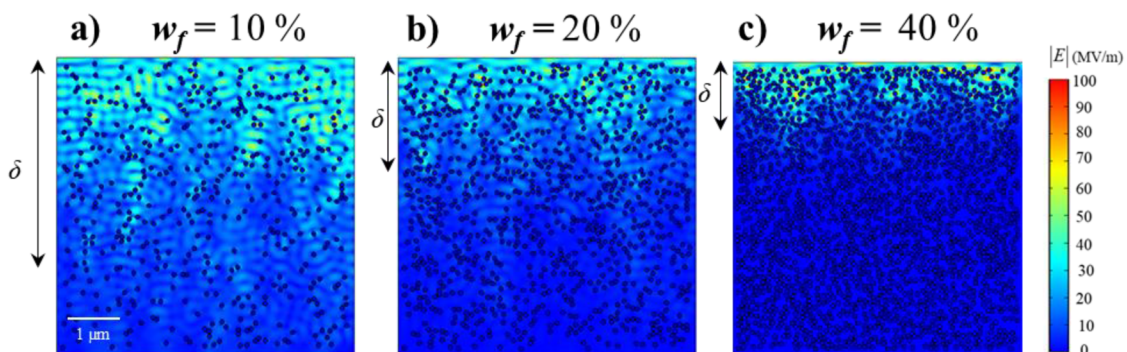

FIG. 3. Electric field magnitude in samples with solids loadings of (a) 10%, (b) 20%, and (c) 40%.

tions of nAl particles). Higher particle concentrations lead to smaller inter-particle distances and closer particle clustering. The resulting effects are two-fold. The first effect is that the eddy current in the particles provides stronger shielding to the incoming EM wave, increasing the reflection and decreasing the wave propagation into the material. As a result, shallower depths of field penetration and heating are seen. The second effect is that the E-field levels near the surface are higher as wave interactions are more localized. The more closely spaced particles trap the waves and cause areas between the particles to experience higher E-field levels. The higher E-field also leads to higher eddy current in the particles, leading to more intense heating.

The thickness of the surface layer in which significant E-field is observed is known as the skin depth (δ), as denoted in Fig. 3. This layer contains the bulk of the current induced and, consequently, the bulk of the heating in the material. The skin depth is commonly defined as the depth where the wave's amplitude reduces to e^{-1} or ~33% of the amplitude at the material surface. Figures 4(a)–4(c) show the averaged electric field magnitude as a function of depth into the material for each solids loading for wavelengths of 266, 532, and 1064 nm, respectively. The skin depth is marked by the horizontal dash line. Several factors, including the electric conductivity σ and the wave frequency f (or wavelength), affect the skin depth.[9] For example, for the material with 15 wt. % solids loading, $\delta = 1.8 \ \mu m$ for the wavelength of 532 nm and $\delta = 2.9 \ \mu m$ for the wavelength of 1064 nm.

The total energy deposited (Q) is calculated using Eq. (5). It can be seen from Fig. 4(d) that the energy deposited is highest when the solids loading is near 20–25 wt. % and is lower at both higher and lower solids loadings. This absorbency trend reflects the outcome of the competing effects of wave penetration and reflection. Specifically, higher solids loadings of nAl lead to higher current and more reflection, resulting in shallower penetration and lower energy dissipation in the material. On the other hand, higher current in the particles leads to more intense conductive heating. Wavelength has a clear impact on the overall absorption. Specifically, the energy absorbed is lower at 266 nm than at 532 and 1064 nm. Among the three mechanisms of energy deposition [conductive, dielectric, and magnetic, see Eq. (4)], conductive heating is dominant for the analyzed materials, accounting for ~90% of the heat generated, followed by ~8% from dielectric heating and only ~2% from magnetic heating. This is expected for the range of wavelength and high conductivity particles.[18] Although Fig. 4(e) shows the heating rate only for a specific laser intensity, a range of laser intensity is considered. It is found that the deposited heat energy Q is proportional to E^2, with $E \approx I_0^{0.5}$.

Temperature increase

The evolution of the resulting temperature increase for a solids loading of 20 wt. % can be seen in Fig. 5. At higher solids loadings, energy deposition and subsequent heating are limited to within a few micrometers of the top surface. The mechanism responsible for this trend is the generation of current in the nAl particles that prevents deeper penetration of the EM waves. Specifically, as the fraction of nAl particles increases, current flow increases near the surface.
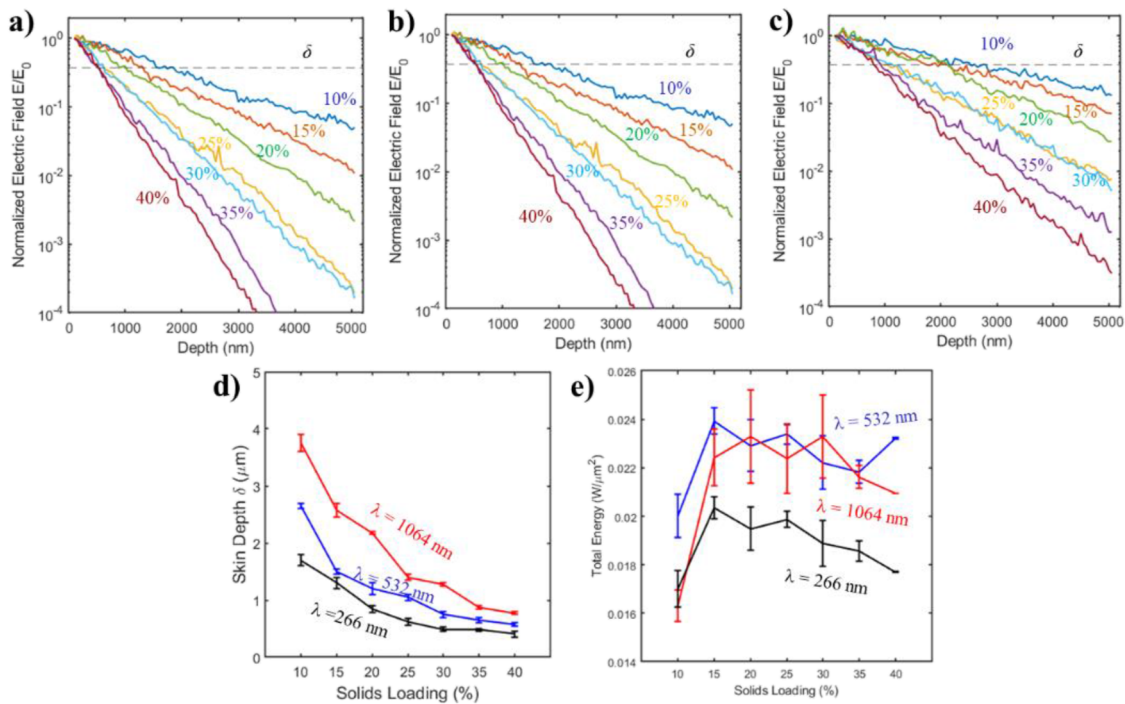

FIG. 4. (a)–(c) Normalized electric field intensity as a function of depth into the material: (a) λ = 266 nm, (b) λ = 532, and (c) λ = 1064 nm. (d) The skin depth as a function of solids loading at different wavelengths. (e) The overall heat deposited into the material per unit surface area of laser incidence for a laser intensity of 1 J/cm^2.
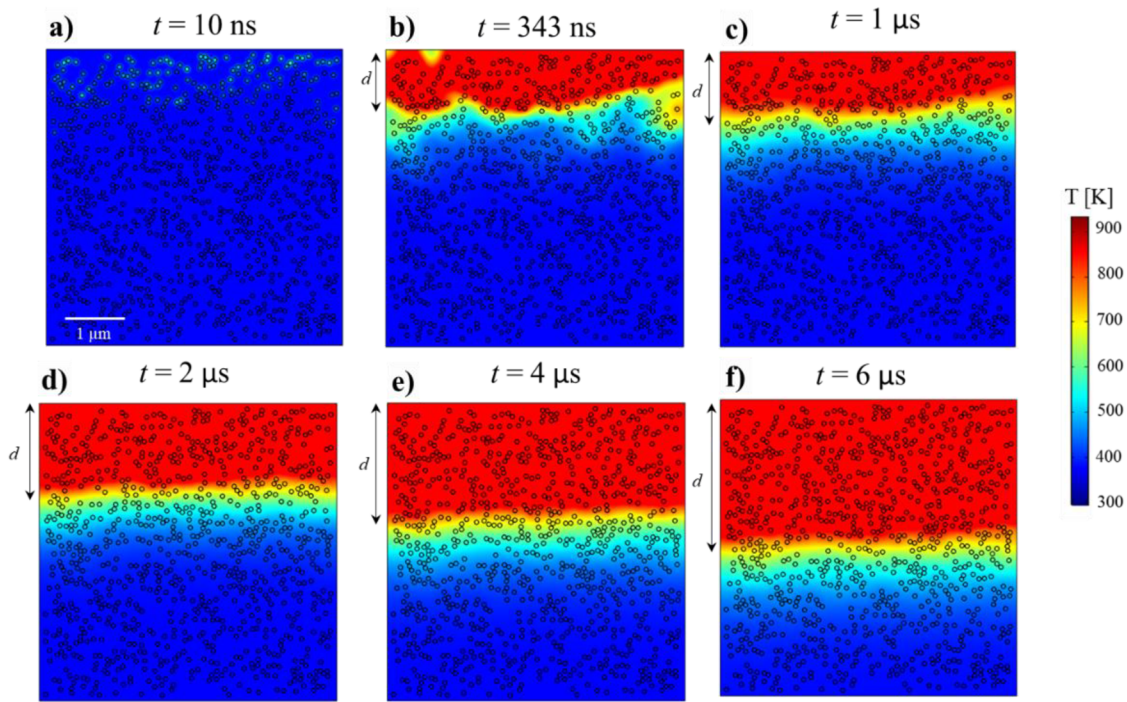
FIG. 5. Temperature increase through time for a sample with a solids loading of 20 wt. % and an incident intensity of I_0 = 1 J/cm². The heated layer thickness d is outlined.

The consequence is two-fold: (1) the increased current near the surface increases Joule heating near the surface, and (2) this increase in current also increases shielding and reflection that prevent further penetration of the EM wave deeper into the material. For most solids loadings, the temperature increase deeper into the material is governed by thermal diffusivity, which is considered in the calculations. In order to quantify the temperature increase and compare the effects of thermal diffusivity, the quantity "penetration depth" (d) is defined as the depth into the material where the average temperature T is above 900 K, as illustrated in Fig. 5. This temperature was chosen as it is the ignition temperature for aluminum nanoparticles.[19,20] In the discussions to follow, this depth is also referred to as the thickness of the heated surface layer.

The temperature fields at t = 20 μs for materials with different solids loadings are compared in Fig. 6. The results for wavelengths of 266, 532, and 1064 nm are shown. Overall, for all solids loadings, the highest temperatures occur at the wavelength is 532 nm. At solids loadings below 20 wt. %, the temperature increases are slightly higher for 266 nm than for 1064 nm, and the opposite is seen at solids loading higher than 20 wt. %. The wavelength also has an effect on the depth of significant temperature increase, which is consistent with the E-field penetration discussed previously. Specifically, the higher wavelengths correspond to higher temperature increases deeper into the material. Note also that the Al particles have much higher thermal diffusivity than the polymer. Therefore, higher solids loading leads to more uniform temperature distributions and is conducive to heating deeper into the material.

The effect of solids loading on the average temperature can be seen in Fig. 7(a). The result shown is for all three wavelengths, but only for three solids loadings, 10, 20, and 40 wt. %. Clearly, the average temperature increases with wavelength and laser intensity, with the temperature for 10 and 40 wt. % at a wavelength of 266 nm significantly lower than that for the higher wavelengths. This is consistent with the experimental observation that the material is difficult to ignite at the 266 nm wavelength, as reported above. This trend is due to the reflection of significant portions of the electromagnetic wave at lower wavelengths, reflecting the plasmonic effect.

The average temperature increase ΔT_{ave} as a function of laser intensity I and time t is quantified using a power law function in the form of

$$
\begin{aligned}
\Delta T_{ave} = \big(&7.86 + 0.025\lambda - 0.42w_f - 1.8 \cdot 10^{-5}\lambda^2 + 1.62 \cdot 10^{-3}\lambda w_f \\
&- 4.19 \cdot 10^{-3}w_f^2 - 8.69 \cdot 10^{-7}\lambda^2 w_f - 5.46 \cdot 10^{-6}\lambda w_f^2 \\
&+ 8.37 \cdot 10^{-5}w_f^3\big)\frac{I}{I_0}\frac{t}{t_0},
\end{aligned} \tag{6}
$$

where I is measured in J/cm² and t is measured in μs. The values of I_0 and t_0 are 0.5 J/cm² and 1 μs, respectively. Note that for solids loading above 20 wt. %, the difference in the constants for the three wavelengths is not insignificant. This reinforces two experimental observations. First, solids loadings greater than 20 wt. % showed similar energy requirements for ignition. Second, there is little
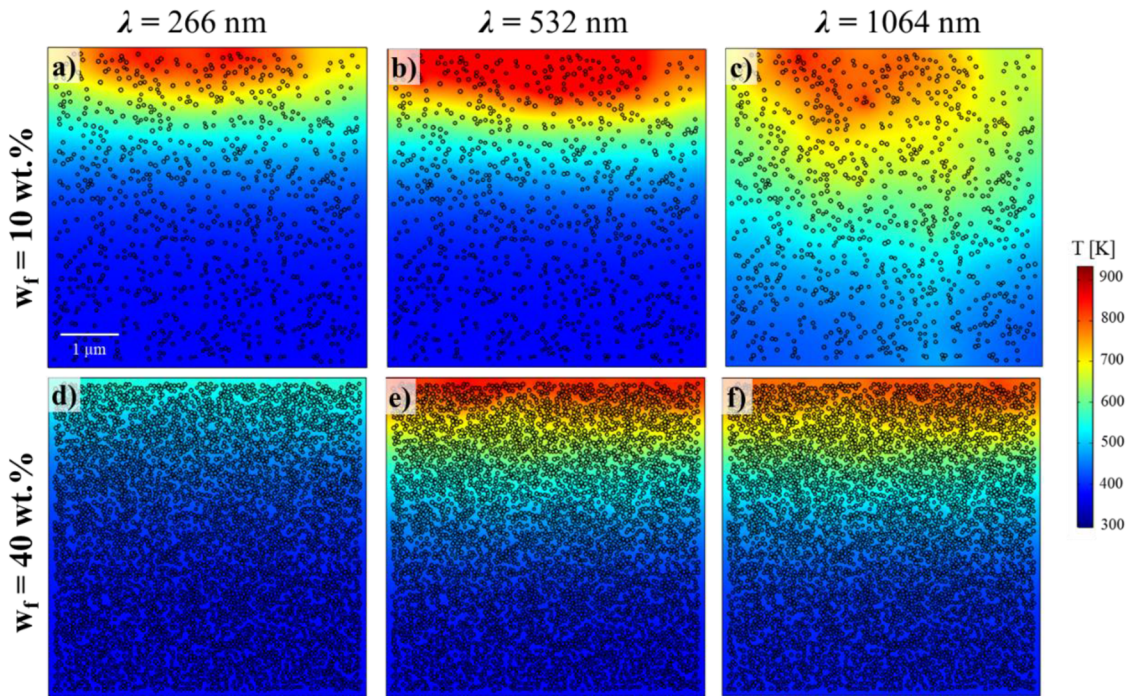
FIG. 6. Comparison of the temperature fields at $t = 20$ μs in the two materials with the lowest (10 wt. %) and highest (40 wt. %) solids loadings considered. The incident laser intensity is $I_0 = 0.5$ J/cm^2. (a) 10 wt. %, $\lambda = 266$ nm; (b) 10 wt. %, $\lambda = 532$ nm; (c) 10 wt. %, $\lambda = 1064$ nm; (d) 40 wt. %, $\lambda = 266$ nm; (e) 40 wt. %, $\lambda = 532$ nm; (f) 40 wt. %, $\lambda = 1064$ nm.

difference in the ignition behavior of the materials at 532 and 1064 nm wavelengths.

While the skin depth δ concerns the depth of E-field penetration into the material and the penetration depth (or thickness of the heated surface layer) d concerns heating, they are closely related. Figure 7(b) shows d as a function of time t for the three wavelengths analyzed. Clearly, low solids loadings and longer wavelengths are not conducive to heating. On the other hand, higher
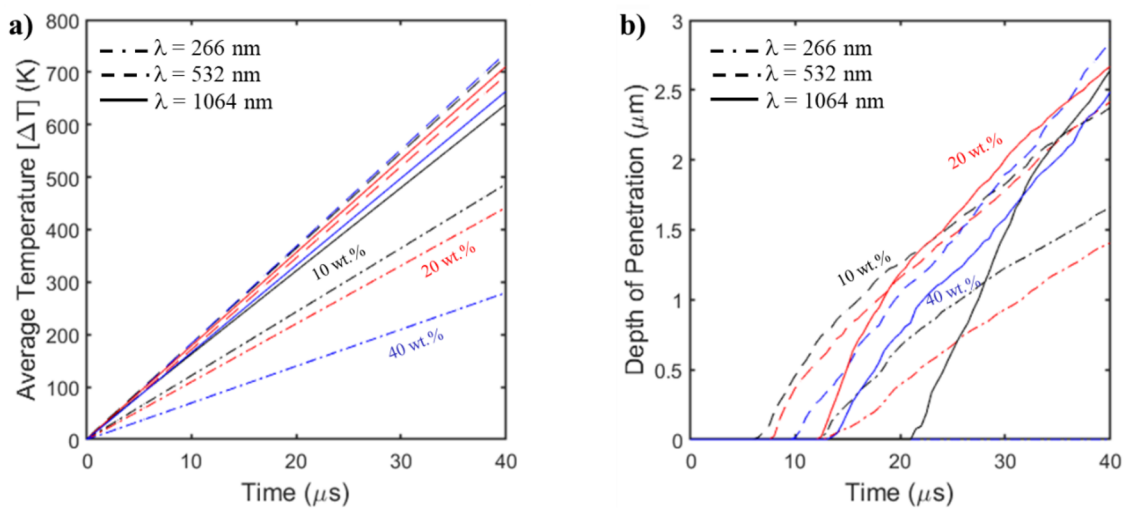

FIG. 7. (a) Average temperature for 10, 20, and 40 wt. % when $I = 0.6$ J/cm^2. (b) Thickness of the heated surface layer d at $I = 0.5$ J/cm^2 for the three wavelengths.

solids loading and longer wavelengths offer avenues for enhancing heat penetration. Although it requires a higher intensity to ignite, the 10 wt. % case's penetration depth increases more rapidly with higher solids loading. The 10 wt. % shows a significant jump in penetration depth while it is still within the skin depth δ, but beyond δ, the increase in d is at a similar trend to the other solids loadings.

To delineate the effect of thermal conduction, two sets of calculations are carried out: one set with the actual thermal conductivities for the constituents and the other set with the conductivities taken as zero. The results are shown in Fig. 8. In both cases, wave and heat penetration decreases with solids loading. Without thermal conduction, heating occurs essentially entirely in the particles. This is due to the fact that Joule heating that occurs only in the particles [first term in Eq. (4)] is dominant. Two observations can be made. First, thermal conduction plays an important role by allowing the heat deposited into the particles to be conducted into the polymer, resulting in overall heating in the composite. Second, solids loading affects the depth of wave and heat penetration. Specifically, at the lowest solids loading (10 wt. %), the particles are sparsely populated, allowing the EM waves to propagate deeper into the material and deposit energy into the particles at deeper depths. However, because there are few particles, the average temperature at each depth is lower (as there are more polymer than particles), resulting in depth of heating (d) lower than the skin depth (δ). As solids loading increases, d increases relative to δ due to conduction. As a result, $d \approx \delta$ at 20 wt. %, and ultimately, $d > \delta$ at 40 wt. %.

The effect of laser intensity and time on the penetration depth d is can be described using

$$d = 3527.6\left(1.21 - 5 \cdot 10^{-4}\lambda - 0.045w_f + 1.24 \cdot 10^{-5}\lambda w_f \right.$$
$$\left. + 4.76 \cdot 10^{-4}w_f{}^2\right)\sqrt{\frac{I}{I_0}} + 2.12 \cdot 10^4\sqrt{D}\left(\frac{t}{t_0}\right)^{0.75}. \quad (7)$$

In the above-mentioned relation, D is the bulk diffusivity in m^2/s, I is measured in J/cm^2, and t is measured in μs. The values of I_0 and t_0 are 1 J/cm^2 and 1 μs, respectively. This equation focuses on the effect of solids loading and diffusivity of the material. Including the adiabatic case mentioned above increases the complexity of this equation, but the trend will follow that shown in the first term of the equation. The differences between wavelengths are most significant for the 266 nm wavelength. The relation shows that at higher solids loadings, the applied intensity has a diminished effect on the penetration depth. More particles drastically reduce the power of the incoming wave within a short distance from the top of the material. Increasing the intensity does not have a direct effect. In samples with less aluminum, there are particles that still receive some energy from the incident wave, just not a significant amount. Increasing the intensity would then increase the amount of energy those particles receive. A higher aluminum content also increases the diffusivity of a sample. This allows a solids loading of 40 wt. % to have similar penetration depths to the 20 wt. % case. However, increasing the diffusivity significantly increases the penetration depth. The
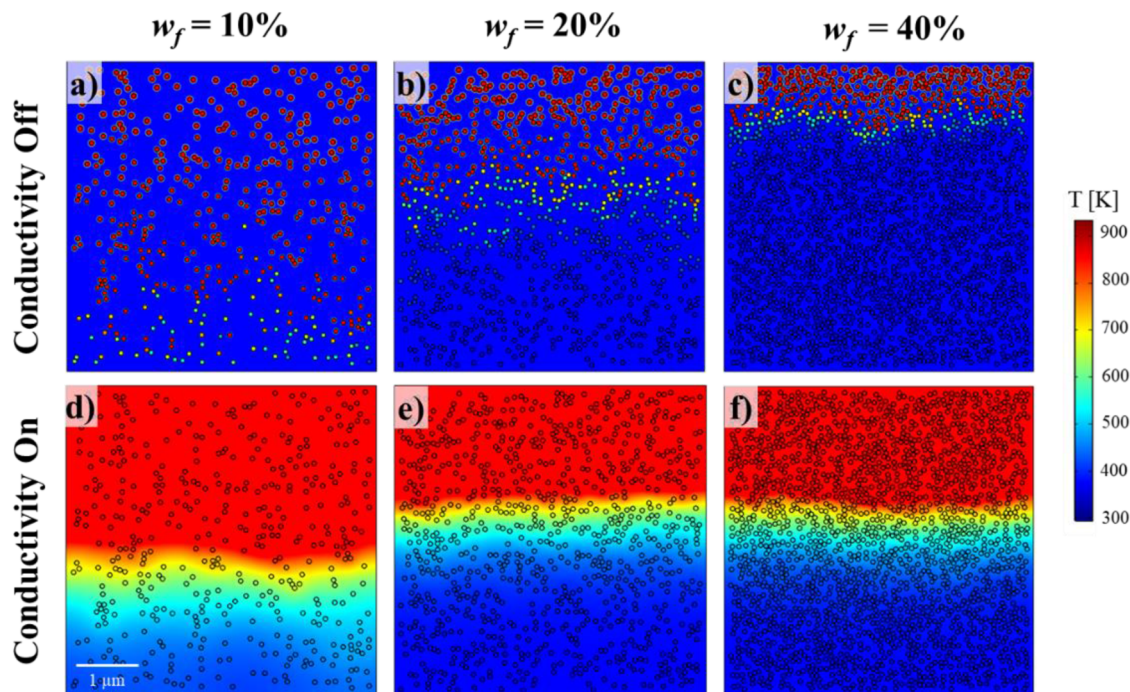
FIG. 8. Comparison of temperature distributions at $t = 8$ μs without [(a)–(c)] and with [(d)–(f)] thermal conduction at three solids loadings. The wavelength is $\lambda = 532$ nm.

interaction between skin depth and penetration depth is further analyzed to provide an understanding of the competition in ignition trends.

Minimum ignition energy and heating rate comparison

The interactions between EM waves and particles and the occurrence of heat transfer and temperature increase, which are important for the laser ignition of nAl/PVDF films, have been analyzed above. Here, the trend in the results is compared with the ignition trend observed in experiments. The hope is to identify correlations, explain mechanisms, and potentially make predictions about ignition using the trend stated above. The quantity of interest is the minimum ignition energy (MIE) or the minimum laser input energy required for ignition. The focus is on the temperature increase and distribution for each solids loading, accounting for the effects of EM wave interaction and thermal diffusivity. In Fig. 4(e), the energy absorbed per unit area Q of laser incidence for an intensity of 1 J/cm^2 is shown. To estimate the MIE and compare with experiments, the empirical criterion of $Q = Q_{cr}$ is used here. It is found that $Q_{cr} = 0.02$ J/μm^2 provides the best fit, as shown in Fig. 9. The predicted trend closely matches that observed in experiments for most solids loading, except at the lowest level of 10%. It is first noted that there is a higher degree of uncertainty in the experimental data for 10% due to challenges in precisely determining the go/no-go threshold. More experiments are needed to accurately address this issue. The computational underestimation of the MIE at the lowest solids loading of 10% may also be partly influenced by many other factors. The primary reason may be associated with the initiation and propagation of reaction, which are two critical steps for successful ignition. Specially, heating and reaction initiate at or around the interfaces between the nAl particles and PVDF. The propagation of reaction throughout the microstructure is required for ignition or what is referred to as a "go" event. At low solids loadings, while initiation can happen in a similar manner to

higher solids loading, propagation is more difficult as the interparticle spacings are higher and exceed the effective range of Al transport through diffusion and advection. This can be a topic of a future study.

On the other hand, computational models currently in development that explicitly account for the chemical reactions should also help shed more light in the near future in a separate publication. The result here shows qualitatively that the relative changes in EM wave penetration/absorption and reflection with solids loading are consistent with the ignition trend, therefore confirming that the underlying mechanism is the competition between wave penetration and reflection.

Overall the predictions show agreement with the experimental results.[1] There are no MIE experimental measurements for the 266 wavelength due to the fact that no ignition was observed in all solids loadings for applied intensities of 0.8 J/cm^2. The heating analysis carried out above shows that it is indeed harder to ignite using this lower wavelength. It is worthwhile to note that the calculated heating trend seems to suggest that the highest solids loadings would be much harder to ignite while the lowest solids loading may overlap with the two higher wavelengths. Only further experiments (which require much higher laser power) can confirm or invalidate this prediction.

SUMMARY AND CONCLUSIONS

A mesoscale model has been developed for studying the interactions between laser-frequency electromagnetic waves and heterogeneous microstructures consisting of dielectric and conductive constituents. The primary focus is on heating and temperature increase resulting from energy dissipation associated with the interactions. The heating mechanisms accounted for are Joule heating, dielectric heating, and magnetic induction heating. The analyzed material of interest is a composite system consisting of nAl particles embedded in a PVDF polymer. The analyzed conditions track those of experiments involving laser illumination over a range of frequency and resulting in ignition in the material, which indicates a self-sustained chemical reaction between nAl and PVDF. A series of calculations are carried out using sets of samples for composites with a range of compositions, as measured by the weight fraction of nAl, which is referred to as solids loading.

Through the evaluation of the EM wave penetration into the material, temperature distribution and increases, and energy deposited, a relationship is established between the heating/energy deposition in the material and the solids loading, accounting for the competing effects of wave transmission/propagation into and reflection away from the material. It is shown that there is an optimum composition (or solids loading) range for maximized heating and energy deposition. This optimum range is ~20 to 30 wt % of nAl, which straddles the stoichiometric composition of ~20 to 25 wt %. This optimum range coincides with the "easiest" composition range for ignition observed in experiments, as measured by the minimum amount of laser input energy required to cause ignition (which is referred to as the "MIE" or minimum input energy). The calculated energy deposition is used to obtain a prediction for the MIE via the use of an empirical ignition criterion, which assumes that ignition occurs when the deposited total heat energy reaches a critical
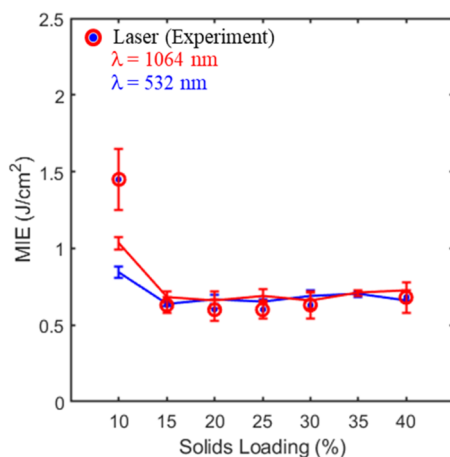

FIG. 9. Comparison of experimentally measured MIE and calculated MIE using a critical energy deposition density of $Q_{cr} = 0.02$ J/μm^2.

value. In the analysis carried out, this critical value is chosen to yield the best match with the experimentally measured MIE. Independent future analyses are required to establish the critical value and factors influencing it. To this effect, a parallel effort is underway to establish a mesoscale model that explicitly resolves the reaction process between the constituents. It is hoped that more insightful results will be reported in a future publication. However, the analyses reported in the current paper have yielded the following results: (1) quantifications of the heat deposition, EM wave penetration depth, thickness of the heated layer of material as functions of laser intensity, solids loading, and time for the studied material system; (2) delineation of the effects of wave penetration and reflection on the heating over a range of material composition or solids loading; (3) elucidation of the variation in the energy deposited as a function of solids loading as the underlying mechanism determining the ignition trend observed in experiments. Another insight obtained is that for the conditions analyzed, Joule heating is by far the dominant heating mechanism, accounting for ~94.5% of the total heat generated, with dielectric heating and magnetic heating making up ~5.5% and ~0%, respectively.

Finally, it is worthwhile to note that while a specific material is analyzed here, the model and approach developed apply to other material systems as well. Ultimately, analyses enabled by this tool set can be used to develop new energetic materials with tailored ignition attributes.

ACKNOWLEDGMENTS

AUTHOR DECLARATIONS

Conflict of Interest

The authors have no conflicts to disclose.

Author Contributions

Daniel Olsen: Data curation (equal); Investigation (lead); Methodology (lead); Writing – original draft (equal). **Kyle Uhlenhake**: Data curation (equal). **Mateo Gomez**: Data curation (equal). **Metin Örnek**: Data curation (equal); Supervision (equal). **Steven F. Son**: Data curation (equal). **Min Zhou**: Supervision (equal); Writing – original draft (equal).

DATA AVAILABILITY

The data that support the findings of this study are available from the corresponding author upon reasonable request.

REFERENCES

[1] K. E. Uhlenhake, D. Olsen, M. Gomez, M. Örnek, M. Zhou, and S. F. Son, "Photoflash and laser ignition of full density nano-aluminum PVDF films," Combust. Flame **233**, 111570 (2021).

[2] W. Kort-Kamp, N. L. Cordes, A. Ionita, B. B. Glover, A. H. Duque, W. L. Perry, B. M. Patterson, D. A. R. Dalvit, and D. S. Moore, "Microscale electromagnetic heating in heterogeneous energetic materials based on x-ray computed tomography," Phys. Rev. Appl. **5**, 044008 (2016).

[3] W. L. Perry and A. L. H. Duque, "Micro to mesoscale temperature gradients in microwave heated energetic materials," J. Appl. Phys. **116**, 054911 (2014).

[4] Z. Alibay, D. Olsen, P. Biswas, C. England, F. Xu, P. Ghildiyal, M. Zhou, and M. R. Zachariah, "Microwave stimulation of energetic Al-based nanoparticle composites for ignition modulation," ACS Appl. Nano Mater. **5**, 2460 (2022).

[5] J. E. Abboud, X. Chong, M. Zhang, Z. Zhang, N. Jiang, S. Roy, and J. R. Gord, "Photothermally activated motion and ignition using aluminum nanoparticles," Appl. Phys. Lett. **102**, 023905 (2013).

[6] X. Chong, J. Abboud, and Z. Zhang, "Plasmonics resonance enhanced active photothermal effects of aluminum and iron nanoparticles," J. Nanosci. Nanotechnol. **15**, 2234 (2015).

[7] R. Malureanu and A. Lavrinenko, "Ultra-thin films for plasmonics: A technology overview," Nanotechnol. Rev. **4**, 259 (2015).

[8] X. Chong, N. Jiang, Z. Zhang, S. Roy, and J. R. Gord, "Plasmonic resonance-enhanced local photothermal energy deposition by aluminum nanoparticles," J. Nanopart. Res. **15**, 1678 (2013).

[9] S. Biswas, I. Arief, S. S. Panja, and S. Bose, "Electromagnetic screening in soft conducting composite-containing ferrites: The key role of size and shape anisotropy," Mater. Chem. Front. **1**, 2574 (2017).

[10] R. Ram, D. Khastgir, and M. Rahaman, "Electromagnetic interference shielding effectiveness and skin depth of poly(vinylidene fluoride)/particulate nano-carbon filler composites: Prediction of electrical conductivity and percolation threshold," Polym. Int. **68**, 1194 (2019).

[11] X. Jin, S. Li, Y. Yang, and X. Huang, "Comparison on laser ignition and combustion characteristics of nano- and micron-sized aluminum," Combust. Sci. Technol. **193**, 341 (2021).

[12] Y. Ohkura, P. M. Rao, and X. Zheng, "Flash ignition of Al nanoparticles: Mechanism and applications," Combust. Flame **158**, 2544 (2011).

[13] C. Crane, M. Pantoya, B. Weeks, and M. Saed, "The effects of particle size on microwave heating of metal and metal oxide powders," Powder Technol. **256**, 113 (2014).

[14] X.-M. Meng, X.-J. Zhang, C. Lu, Y.-F. Pan, and G.-S. Wang, "Enhanced absorbing properties of three-phase composites based on a thermoplastic-ceramic matrix ($BaTiO_3$ + PVDF) and carbon black nanoparticles," J. Mater. Chem. A **2**, 18725 (2014).

[15] W. Zhou, J. Zuo, and W. Ren, "Thermal conductivity and dielectric properties of Al/PVDF composites," Compos., Part A **43**, 658 (2012).

[16] Q. Chen, H. Qi, Y.-T. Ren, J.-P. Sun, and L.-M. Ruan, "Optical properties of truncated Au nanocages with different size and shape," AIP Adv. **7**, 065115 (2017).

[17] M. A. Trunov, M. Schoenitz, and E. L. Dreizin, "Ignition of aluminum powders under different experimental conditions," Propellants, Explos., Pyrotech. **30**, 36 (2005).

[18] P. Biswas, G. W. Mulholland, M. C. Rehwoldt, D. J. Kline, and M. R. Zachariah, "Microwave absorption by small dielectric and semi-conductor coated metal particles," J. Quant. Spectrosc. Radiat. Transfer **247**, 106938 (2020).

[19] A. Rai, D. Lee, K. Park, and M. R. Zachariah, "Importance of phase change of aluminum in oxidation of aluminum nanoparticles," J. Phys. Chem. B **108**, 14793 (2004).

[20] A. Starik, A. Savel'ev, and N. Titova, "Specific features of ignition and combustion of composite fuels containing aluminum nanoparticles (Review)," Combust., Explos. Shock Waves **51**, 197 (2015).